Global and Planetary Change 178 (2019) 184–192

Contents lists available at ScienceDirect

Global and Planetary Change

journal homepage: www.elsevier.com/locate/gloplacha

Dry/wet pattern changes in global dryland areas over the past six decades

Yupeng Li[a,b], Yaning Chen[a,*], Zhi Li[a]

[a] State Key Laboratory of Desert and Oasis Ecology, Xinjiang Institute of Ecology and Geography, Chinese Academy of Sciences, Urumqi 830011, China
[b] University of Chinese Academy of Sciences, Beijing 100049, China

ARTICLE INFO

Keywords:
Climate change
Dryland areas
P/PET

ABSTRACT

As reported in previous studies, global warming has caused a clear uptick in dryland areas since the 1950s. Meanwhile, the accelerated expansion of drylands has become particularly evident over the past 40 years, with dry/wet patterns showing significant differences prior to and after 1980. This paper uses the Precipitation/Potential evaporation (P/PET) index to analyze changes occurring in the dry/wet structure of various spatial and temporal scales during 1948–2008. The results show the emergence of complex aridity changes on a regional scale. While aridity generally decreased in the drylands of Asia during 1948–2008, the change in aridity was opposite in the drylands of the American and African continents between 1948 and 1979 and 1980–2008. Specifically, drylands in the American continent showed a wetting tendency during 1948–1979 and a drying tendency during 1980–2008, whereas drylands in the African continent underwent significant drying during 1948–1979 followed by subtle wetting in 1980–2008. Even though rapid warming since the 1980s has become an increasingly important cause of the recent global drying trend, especially in East and Central Asia, the changes in aridity in the American and African drylands is attributable to natural variabilities in precipitation associated with multi-decadal surface sea temperature changes, along with large-scale circulation patterns.

1. Introduction

Globally, drylands (defined as regions with P/PET of < 0.65) occupy approximately 41% of terrestrial land surfaces and are home to > 38% of the world's population. Around 90% of current drylands are located in developing countries (Huang et al., 2015a). Due to their fragile ecological environment, low soil fertility and scarce precipitation, drylands are extremely sensitive to degradation caused by human activities and climate warming (Feng and Fu, 2013; Huang et al., 2015a; Reed et al., 2012). Research indicates conflicting ideas on how dryland areas respond to climate change. In studies based on either observations or model simulations, researchers found that aridity has increased globally since around 1950, indicating a drying trend that may continue well into the 21st century due to global warming (Feng and Fu, 2013; Huang et al., 2015a). However, other recent studies on global aridity trends since 1948 concluded that while some regions have become more arid and others less so, there has been little overall change in terms of global averages and little to no obvious trend in aridity in global drylands (Greve et al., 2014). These contradictory conclusions could originate from issues with the ET baseline period and precipitation data sets (Trenberth et al., 2014). Despite obtaining opposing results about the overall aridity trend of drylands, they all acknowledge there is a clear spatial heterogeneity in the response of drylands to climate change.

Spatial heterogeneity focuses on aridity changes across different regions and areas as well as across different periods. The projected changes in aridity show decreases in most of the global land surface, except for northern China, India, the southern Saharan, and eastern equatorial Africa. In observing changes in aridity between 1948 and 2008, Feng and Fu (2013) explained that the most prominent drying trends occurred in northern Africa, East Asia, eastern Australia, and southern Europe, whereas a subtle wetting trend occurred in central/western U.S., South America, and Western Australia.

Furthermore, responses to changes of dry/wet structures in dryland areas prior to and after the 1980s show an accelerating increasing trend from 1980 onward. Dai (2011) designated regions with PDSI ≤ 3 as drylands and found that these areas experienced a sharp increase under the combined effects of enhanced warming and reduced precipitation. Global land areas under drought conditions varied between 14% and 16% from 1950 to 1982, when it experienced a sharp jump (by ~ 10%) due to the 1982/83 El Niño. Huang et al. (2015a) using the P/PET to define drylands, also discovered that global drylands had greatly expanded, especially after the early 1980s, with a much slower expansion occurring before that time. In fact, temporal variations in dryland areas

* Corresponding author.
E-mail address: chenyn@ms.xjb.ac.cn (Y. Chen).

https://doi.org/10.1016/j.gloplacha.2019.04.017
Received 19 December 2018; Received in revised form 3 April 2019; Accepted 30 April 2019
Available online 02 May 2019
0921-8181/

are in line with changes in global soil moisture, which present no obvious change prior to 1980 but decline much faster shortly thereafter (Cheng and Huang, 2016). Some regional studies also confirm the existence of this phenomenon. Shi et al. (2007) showed that arid northwestern China has experienced a shift to wetter conditions since the mid-1980s (Shi et al., 2007), while rainfall in the Sahara region decreased before the 1980s, but after that, it showed an increasing trend (Caminade and Terray, 2010).

However, there are still contradictions in the interpretation of this post-1980 sudden shift in dryland areas. Some scholars blame the change on global warming caused by greenhouse gas emissions, whereas others attribute the historical drying trend to decreasing precipitation associated with multi-decadal surface sea temperature (SST) changes (Dai and Zhao, 2016). For example, in the western United States, the Pacific Ocean plays a more important role in controlling precipitation over arid and semi-arid regions. After 1978, the Pacific Decadal Oscillation (PDO) changed from a cold phase to a warm one, which caused below-normal precipitation and led to increased aridity across southwestern North America (Gutzler et al., 2002; Hu and Huang, 2009).

From the above analysis, we can see that the study of dry/wet structure changes in the 1980s is limited to mostly dryland areas. In addition, much of the research connects recent drying trends with global warming but ignores the relationship between climate change in dryland areas and variations in large-scale SST. In light of this gap, the present paper will explore the characteristics of aridity changes in the decades before and after 1980. Our focus will include drylands on a global scale as well as subtypes of drylands and drylands on a regional scale. Our aim is to determine the change mechanisms driving the shifting rates of precipitation and potential evapotranspiration, as well as possible mechanisms instigating climate change in drylands around the world.

2. Data source

In comparing the spatial distributions of drylands identified by annual precipitation, Köppen-Geiger climate classification, surface vegetation types and the P/PET, Huang et al. (2015a) indicated that global drylands defined by P/PET were primarily distributed in the middle and lower latitudes and closely match the map from the United Nations Environment Programme (UNEP). The aridity index (P/PET), which represents the degree of climatic dryness, was defined as the ratio of annual precipitation to annual potential evapotranspiration. Under this quantitative indicator, drylands are defined as regions with P/PET of < 0.65. Drylands are further classified into hyper-arid (P/PET $<$ 0.05), arid ($0.05 \leq$ P/PET < 0.2), semi-arid ($0.2 \leq$ P/PET < 0.5), and dry sub-humid ($0.5 \leq$ P/PET < 0.65) subtypes. In this paper, drylands exclude Antarctica and high latitude regions ($> 60°$N). Moreover, in order to facilitate analysis and show that the effects of atmospheric circulation can vary across different dryland regions, we separate dryland areas into eight different regions as shown in Fig. 1. The eight main drylands regions including East Asia(EAS; 80°E–140°E, 30°N–60°N) , Central Asia (CAS; 40°E–80°E, 30°N–60°N), Northern Africa (NAF; 20°W–40°E, 5°N–30°N), Southern Africa (SAF; 9°E–43°E, 10°S–40°S), East Australia (EA; 139°E–156°E, 10°S–40°S), Central/West Australia (CWA; 110°E–139°E, 10°S–40°S), North America (NAM; 130°W–89°W, 30°N –60°N), and South America (SAM; 77°W–50°W, 30°S–60°S).

The precipitation dataset applied in this study is derived from the National Centers for Environmental Prediction (NCEP) Climate Prediction Center (CPC) (Chen et al., 2002), which is typically referred to as the PRECipitation REConstruction over Land (PREC/L) dataset. The PREC/L is an observation station-based dataset, with a global cover of $0.5° \times 0.5°$ latitude-longitude resolution for the period extending from 1948 to the present. The PREC/L is derived from gauge observations taken at over 17,000 stations and collected from two large individual datasets provided by Global Historical Climatology Network version 2 (GHCN2) and the Climate Anomaly Monitoring System (GHCN + CAMS). It is regularly updated in near real-time by virtue of its many stations and unique interpolation methods.

In contrast to temperature data, precipitation data uncertainty has a greater impact on the results. Compounding this is the general lack of precipitation gauge stations located at higher latitudes ($> 60°$), higher altitudes (e.g., Qinghai-Tibet Plate), and desert areas (e.g., Sahara Desert). Thus, to ensure the accuracy of the results, we chose not to include data from high latitude areas, but instead used data only from equatorial regions. Additionally, to quantify the uncertainty in global precipitation and to better illustrate the reliability of using the PREC/L dataset, the trends in land precipitation were analyzed using a number of datasets, including the Climate Research Unit (CRU) (Mitchell and Jones, 2005), the Global Precipitation Climatology Centre (GPCC) full data reanalysis, version 6 (Schneider et al., 2011), and the University of Delaware dataset (UDel) (Legates and Willmott, 1990). As well, it should be noted that the observed precipitation data for hyper-arid and high-altitude regions may not be reliable due to poor data coverage (Chen et al., 2002).

Data from four circulation indices (the North Atlantic Oscillation [NAO] index, the PDO index, the Atlantic Multi-Decadal Oscillation [AMO] index, and the Niño Regions 3.4 surface sea temperature [Niño 3.4] index) were used to investigate the relationship between dry/wet changes in global drylands and atmospheric circulation patterns. The circulation indexes were downloaded from the climate explorer. These indicators are commonly used in climate change research and their changes have a significant impact on global climate. For example, Trenberth et al. (2014) demonstrated that natural variability, especially El Niño-Southern Oscillation (ENSO), is the primary cause of numerous episodic droughts around the world.

3. Methods

The PET data used in this study were provided by Feng and Fu (2013) and were calculated using the Penman-Monteith method. This approach considers a broad range of meteorological parameters, including net radiation, relative humidity, wind speed, temperature and vegetation characteristics related to the evapotranspiration process. Hence, the PET can be calculated as:

$$PET = = \frac{0.408\Delta(R_n - G) + \gamma \frac{900}{273 + T_{mean}} u_2 (e_s - e_a)}{\Delta + \gamma(1 + 0.34u_2)}$$

where R_n is the net radiation (MJ m^{-2} day^{-1}), G is the heat flux into the ground, T_{mean} is the mean month air temperature at 2 m height, $u_2$is the wind speed at 2 m height, e_s is the saturation vapor pressure, e_a is the actual vapor pressure, $e_s - e_a$ is the vapor pressure deficit, Δ is the slope of the saturation vapor pressure curve, and γ is the psychrometric constant.

In order to calculate PET, wind speed, specific humidity and net radiation (including shortwave and longwave net radiation), reanalysis datasets from the Global Land Data Assimilation System (GLDAS) were used, along with the observed monthly surface air temperature (SAT) dataset. The GLDAS datasets, which start at 1948, have global coverage at a $0.5° \times 0.5°$ latitude-longitude resolution (Rodell et al., 2004). The observed SAT dataset was developed by the National Centers for Environmental Prediction (NCEP)/Climate Prediction Center (Chen et al., 2002). Solar radiation was corrected based on two global radiation products during 1983–2000, and wind and specific humidity were adjusted to the observationally-based climatology developed by the Climate Research Unit (CRU) at the University of East Anglia. The formula as below.

$$[V_{adj}]_{Y,M} = [V]_{Y,M} / [V_{clim}]_M \times [V_{CRU,clim}]_M$$

where $[V]_{Y,M}$ and $[V_{adj}]_{Y,M}$ are the original and adjusted climate

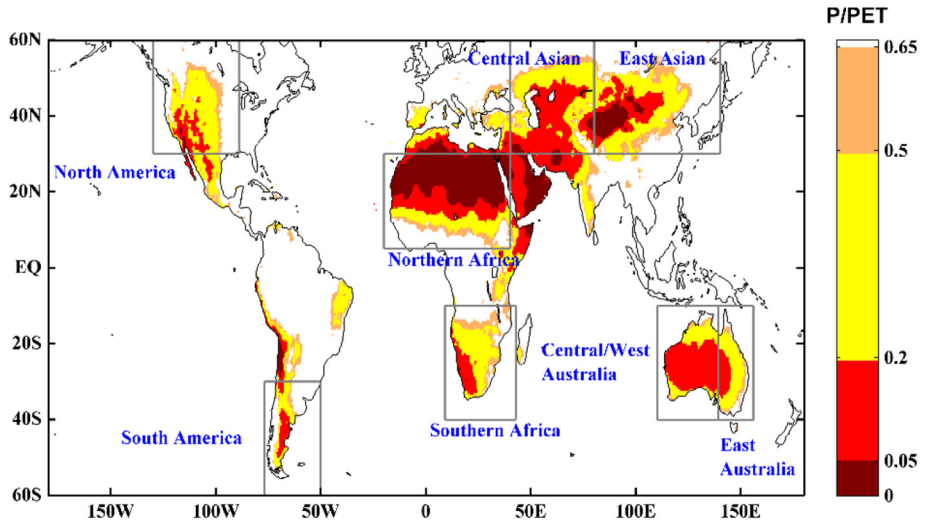

Fig. 1. Distribution of drylands and subtypes (hyper-arid, arid, semi-arid, and dry sub-humid) determined by annual P/PET in 1948–2008. The scope of the eight main drylands regions is also identified. East Asia(EAS; 80°E–140°E, 30°N–60°N) , Central Asia (CAS; 40°E–80°E, 30°N–60°N), Northern Africa (NAF; 20°W–40°E, 5°N–30°N), Southern Africa (SAF; 9°E–43°E, 10°S–40°S), East Australia (EA; 139°E–156°E, 10°S–40°S), Central/West Australia (CWA; 110°E–139°E, 10°S–40°S), North America (NAM; 130°W–89°W, 30°N–60°N), and South America (SAM; 77°W–50°W, 30°S–60°S).

variables (humidity or wind speed) in GLDAS for year Y and month M, respectively. $[V_{clim}]_M$ and $[V_{CRU,\ clim}]_M$ are the 1961–1990 mean values of GLDAS and CRU, respectively.

To ensure that the results are robust and do not depend on the data set used, Feng and Fu (2013) used solar radiation, humidity and wind speed from the Twentieth Century Reanalysis (20CR) datasets to calculate PET. The temperature and precipitation data developed at the University of Delaware were used to calculate P/PET. Therefore, four combinations (i.e., CPC and GLDAS, CPC and 20CR, UDel and GLADS, and UDel and 20CR) were obtained and compared. The results showed good agreement in the global averaged temporal variations of PET. However, the trends were slightly different in certain regions as a result of using individual precipitation datasets. Therefore, in this study, PET was derived from GLDAS, but precipitation data were obtained from multiple datasets.

Trends in annual P/PET, precipitation and potential evapotranspiration were calculated by using the nonparametric Mann-Kendall test (Kendall, 1975; Mann, 1945). A trend was considered statistically significant at a significance level of 95%.

4. Results

4.1. Changes in dry/wet patterns in drylands

The spatial distribution of drylands and the individual components for the climatology of the 1948–2008 timeframe are based on P/PET (Fig. 1). The major hyper-arid areas generally occurred over deserts such as the Rub al Khali Desert in the eastern Arabian Peninsula, the Sahara Desert, and the Taklimakan Desert. Arid areas were mainly located in Central Asia and Australia, and semi-arid and dry sub-humid regions were located outside the hyper-arid and arid regions. The semi-arid regions occupied the largest proportion, accounting for 15% of Earth's land area. Other dry types (hyper-arid, arid, dry sub-humid) occupied 7.5%, 13.0%, and 6.2%, respectively.

Fig. 2 illustrates temporal variations in area change for total drylands during 1948–2008. Since the late 1940s, drylands have increased at a rate of 512,180 km^2/decade. The main feature is the sharp jump in drylands expansion in the 1980s, with the area of drylands increasing 3.1% ($1.90 \times 10^6 km^2$) between 1980 and 2008 compared to 1948–1979. The drying areas covered 62.5% of the world's drylands, showing a significant decline in P/PET in North Africa and East Asia (Fig. 3(a)). Significant drying areas are mainly concentrated in North Africa and East Asia, which are the main area for increased dryland areas; however, significant wetting areas can also be found in North America and Central/West Australia.

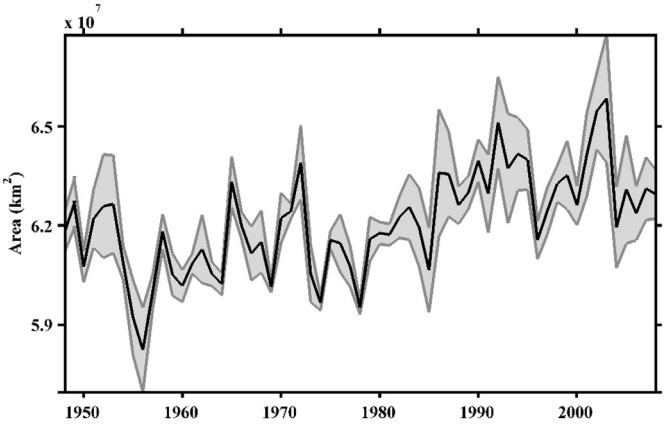

Fig. 2. Temporal variations in area change for total drylands. Uncertainty in precipitation is estimated by four alternative global precipitation data sets.

In comparing the spatial patterns of P/PET trends for the periods 1948–1979 and 1980–2008, we can see that the main differences occurred between drylands in North America and North Africa (Fig. 3(b, c)). Drylands in North America showed slight wetting from 1948 to 1979 but reversed to significant drying after that. The situation is opposite in the drylands of North Africa where, prior to the wetting, there was significant drying in North African drylands during 1948–1979. In East Asia, however, the long-term drought did not noticeably change the drylands over these two periods. Significant drying areas were much higher during 1948–1979 than during 1980–2008. These robust results were also verified by PDSI and SPEI (Fig. S1).

4.2. Changes in dry/wet patterns in dryland subtypes

There was an expansion of hyper-arid, arid, semi-arid and dry sub-humid areas by 2.5% ($2.8 \times 10^5 km^2$), 3.0% ($5.7 \times 10^5 km^2$), 3.6% ($7.8 \times 10^5 km^2$) and 2.9% ($2.6 \times 10^5 km^2$), respectively, from 1980 to 2008 compared to 1948–1979. The largest increase in semi-arid regions accounted for 41.2% of the entire expansion. In contrast, the growth of hyper-arid and arid dryland areas were not very large (Fig. S2), mainly because arid regions declined prior to the 1970s and then increased, owing to the rise in Southern Hemisphere precipitation levels and the subsequent transformation of arid into semi-arid regions (Feng and Fu, 2013). Hyper-arid regions underwent some fluctuations but experienced only slight changes overall.

The drylands subtypes which experienced changes were accompanied by reciprocal transformation. Fig. 4(a) identifies areas where

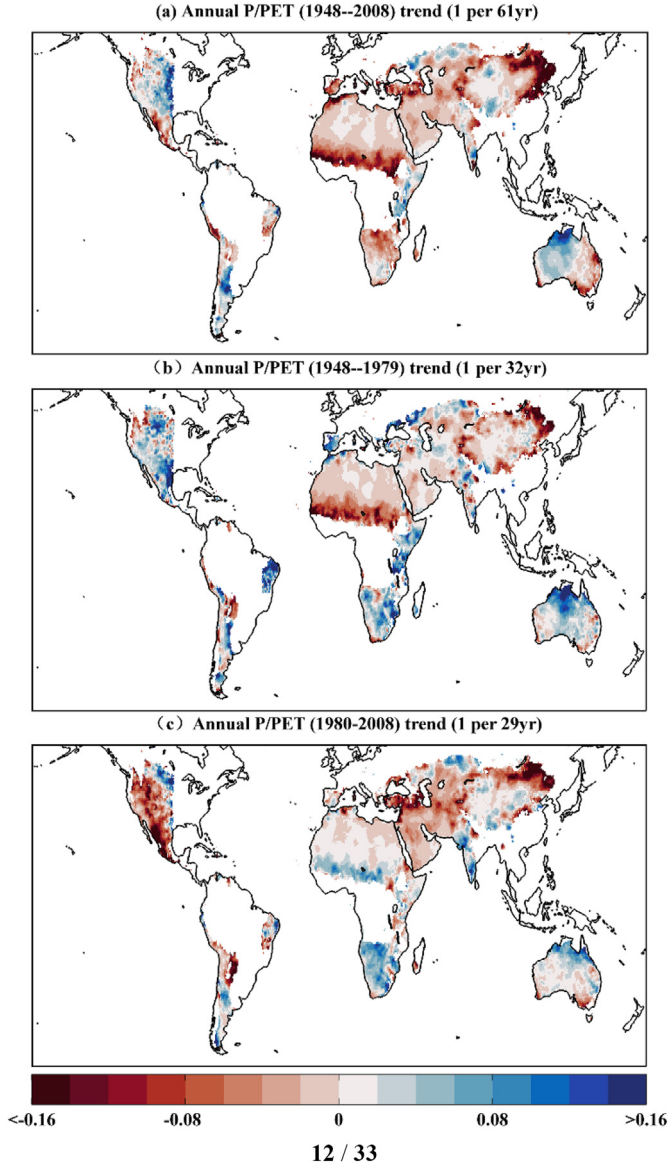

Fig. 3. Global drylands distribution of the linear trend of P/PET (a) for 1948–2008 (b) for 1948–1979 (c) for 1980–2008.

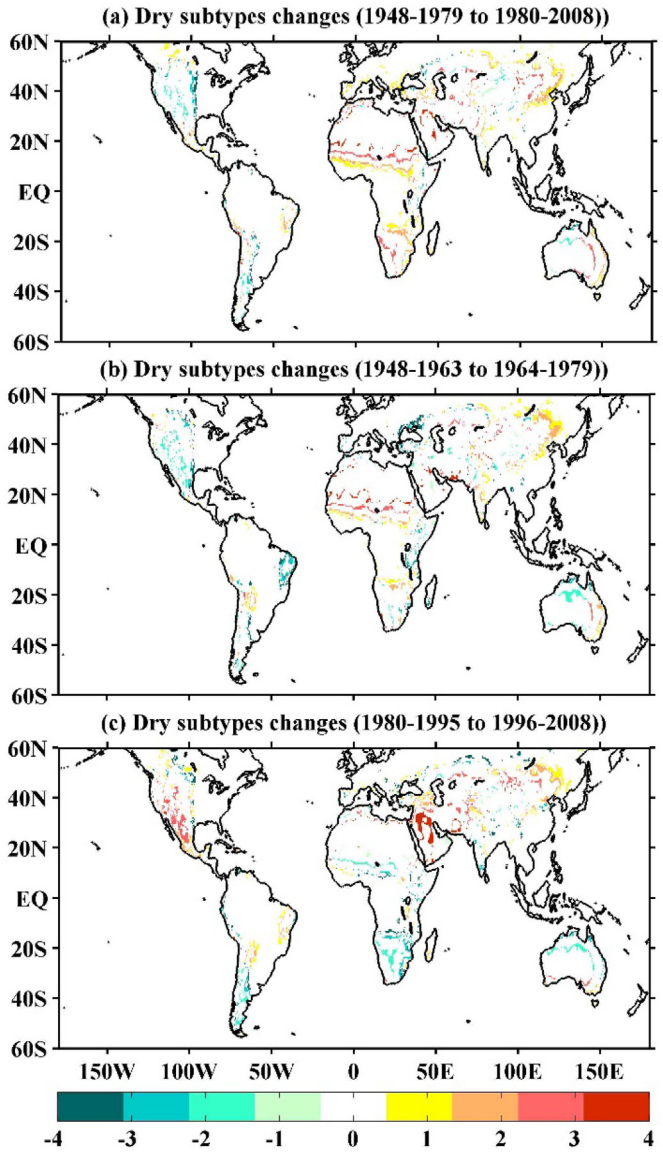

Fig. 4. Global distribution of neighboring dry subtype changes (a) during 1980–2008 relative to 1948–1979 (b) during 1964–1979 relative to 1948–1963 (c) during 1996–2008 relative to 1980–1995. -4 to 4 respectively represent Dry subhumid to humid, Semiarid to dry subhumid, Arid to semiarid, Hyper-arid to arid, Humid to dry subhumid, Dry subhumid to semiarid, Semiarid to arid and Arid to hyper-arid.

drought types changed during 1948–2008, showing that the region's growing drier accounted for about 4.58% of the global land area and were mainly located in Northeast China and tropical Africa. In contrast, the regions which grew wetter occupied only 1.27% of the global land area and were mainly located on the American continent and northern Australia. The increase in drier regions primarily ensued from conversions of dry sub-humid regions into semi-arid ones, and from humid regions into dry sub-humid ones. Decreases in arid and dry sub-humid regions were the main reason for increases in wetter regions (Fig. 5).

During both 1948–1979 and 1980–2008, more areas became drier than wetter (Fig. 5). However, in 1948–1979, the drier areas accounted for 3.16% of the global land mass, whereas in 1980–2008, 3.95% grew wetter as arid areas transformed into semi-arid zones (Fig. 4(b)). The drying trend continued globally during 1980–2008, even though some of the land in the African continent became wetter. The areas which grew wetter during this period occupied 2.15% less of the global land areas that became wetter (2.91%) in 1948–1979. The decrease in wetter regions could be explained by the conversion of dry sub-humid regions into semi-arid ones and humid regions into dry sub-humid ones, mainly in East Asia and America (Fig. 4(c)).

4.3. Changes in dry/wet patterns in drylands across different regions

Changes in dry/wet patterns across different regions showed a geographical uniqueness that was not consistent with changes in drylands overall (Fig. 6). In order to investigate whether the area change was significant for drylands and their subtypes in different regions, we compared the means of dryland areas for both 1948–1979 and 1980–2008 using the Paired-Samples *t*-test. Results indicate that while drylands in East Asia ($4.87 \times 10^5\,km^2$), Northern Africa ($4.18 \times 10^5\,km^2$) and Southern Africa ($2.90 \times 10^5\,km^2$) significantly expanded, the increases behaved differently in different regions. In East Asia and Southern Africa, the increase mainly came from an expansion of arid and semi-arid regions, while the increase in drylands in Northern Africa mostly resulted from expansions of hyper-arid and arid regions.

Elsewhere in the world, East Australia, Central Asia and North America showed some expansion of their dryland areas, though the

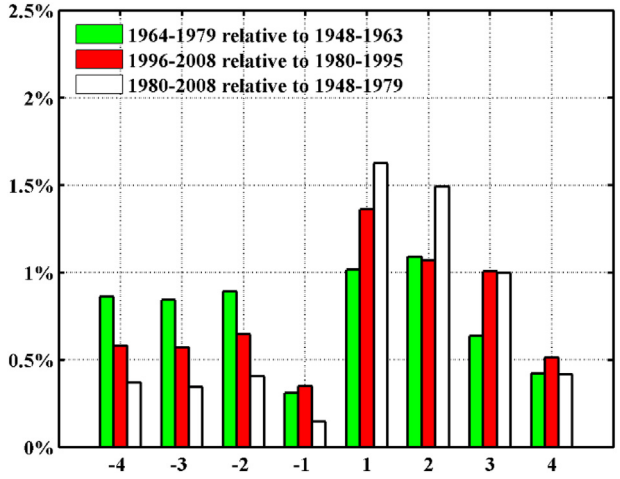

Fig. 5. Neighboring subtype changes during 1964–1979 relative to 1948–1963, during 1996–2008 relative to 1980–1995 and during 1980–2008 relative to 1948–1979. Unit: percentage of global land area. -4 to 4 respectively represent Dry subhumid to humid, Semiarid to dry subhumid, Arid to semiarid, Hyper-arid to arid, Humid to dry subhumid, Dry subhumid to semiarid, Semiarid to arid and Arid to hyper-arid.

growth was not significant. In Central Asia, for instance, the entire area grew drier, but some places grew slightly wetter in the north, which weakened the overall drying trend. In East Australia, the expansion of drylands simply followed a long-term trend, and in North America, the drylands became drier after becoming wetter prior to the 1980s, so there was no obvious change in this region. Meanwhile, the drylands of South America and Central/West Australia decreased slightly, but the reduction was not significant.

4.4. Effects of precipitation and PET on P/PET

Warming-induced increases in evaporation became more and more pronounced across most drylands regions. The results of this study show that, since the late 1940s, the temperature in the drylands increased by 1.2 °C and PET rose sharply at a rate of 5.2 mm/decade. However, overall changes in precipitation were not obvious. In fact, PET in all dryland subtypes, without exception, significantly increased. At the same time, precipitation decreased significantly in semi-arid and dry sub-humid regions at a rate of −4 mm/decade and −6.8 mm/decade, respectively.

Additionally, the spatial structure of P/PET could be explained by the spatial trend of precipitation and potential evaporation (Fig. 7). From 1948 to 2008, the largest increase in drought regions in East Asia, Northern Africa, and Southern Africa were induced by a reduction in precipitation and an increase in evaporation. However, areas that were growing wetter, such as North America and Central/West Australia, experienced a rise in precipitation levels coupled with a decrease in evaporation. The precipitation and potential evaporation structure during 1948–1978 is similar to that of the 1948–2008 period.

During 1980–2008, the climate in the drylands changed, and evaporation levels in Central Asia, East Asia and North Africa significantly increased. Northern Africa, however, owing to enhanced precipitation, counteracted the negative effect of evaporation and became wetter. In North America, as precipitation decreased and evaporation increased, the climate changed from wetting to drying. In contrast, in Southern Africa, the climate changed from drying to wetting due to increased precipitation and weakened evaporation. Meanwhile, precipitation in Australia continued to increase, but as the range was smaller than before, the wetting trend weakened in this period (Fig. S3, Fig. S4).

4.5. Relationship between SST changes and P/PET ratios

Global climate change in dryland areas is affected by global and local factors, such as changes in SST, greenhouse gas emissions and land use (Huang et al., 2015b); it is also affected by interactions between the atmosphere and ocean which controls the surrounding water vapor content. Because P/PET changes in response to global warming might have been controlled by global-scale systems such as the PDO, AMO, NAO and Niño 3.4, we calculated the correlation coefficients of P/PET with PDO, AMO, NAO and Niño 3.4 (Fig. 8).

We noted that PDO changed from a cold to a warm phase after 1978. The distribution of the correlation coefficients between P/PET and PDO exhibited a negative relationship over most of Africa and East Australia, indicating a clear wetting trend in those areas. A significant positive relationship was observed over North America and Central Asia, which means the climate in those areas changed from wet to dry. AMO showed a downward trend before 1980s, followed by an increase. Fig. 8(b) shows the distribution of the correlation coefficients between P/PET and AMO. As can be seen, a significant positive relationship occurred between Northern and Southern Africa, while a significant negative relationship occurred between the Arabian Peninsula and North America. NAO presented a relatively complex change. A positive phase occurred in the 1950s, but the trend became negative in the 1960s. Then, starting from the 1970s, the trend exhibited a positive phase until the 2000s. Most drylands were positively correlated with NAO, except for a few areas (e.g., North Central Asia and Africa near the tropics).

Fig. 8(d) shows the distribution of the correlation coefficients

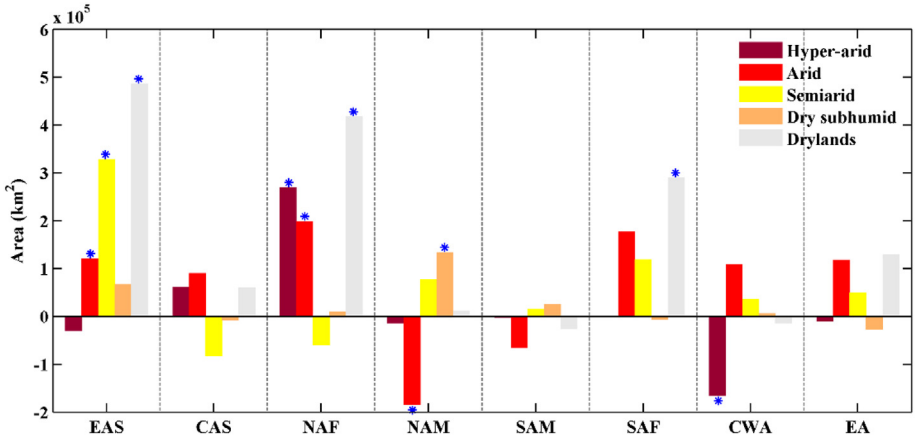

Fig. 6. The area changes by climate type (Hyper-arid, Arid, Semiarid, Dry subhumid and drylands) for 1980–2008 compared to 1948–1979 in the eight main drylands regions. * indicates that significant change in area at the 95% statistical confidence level.

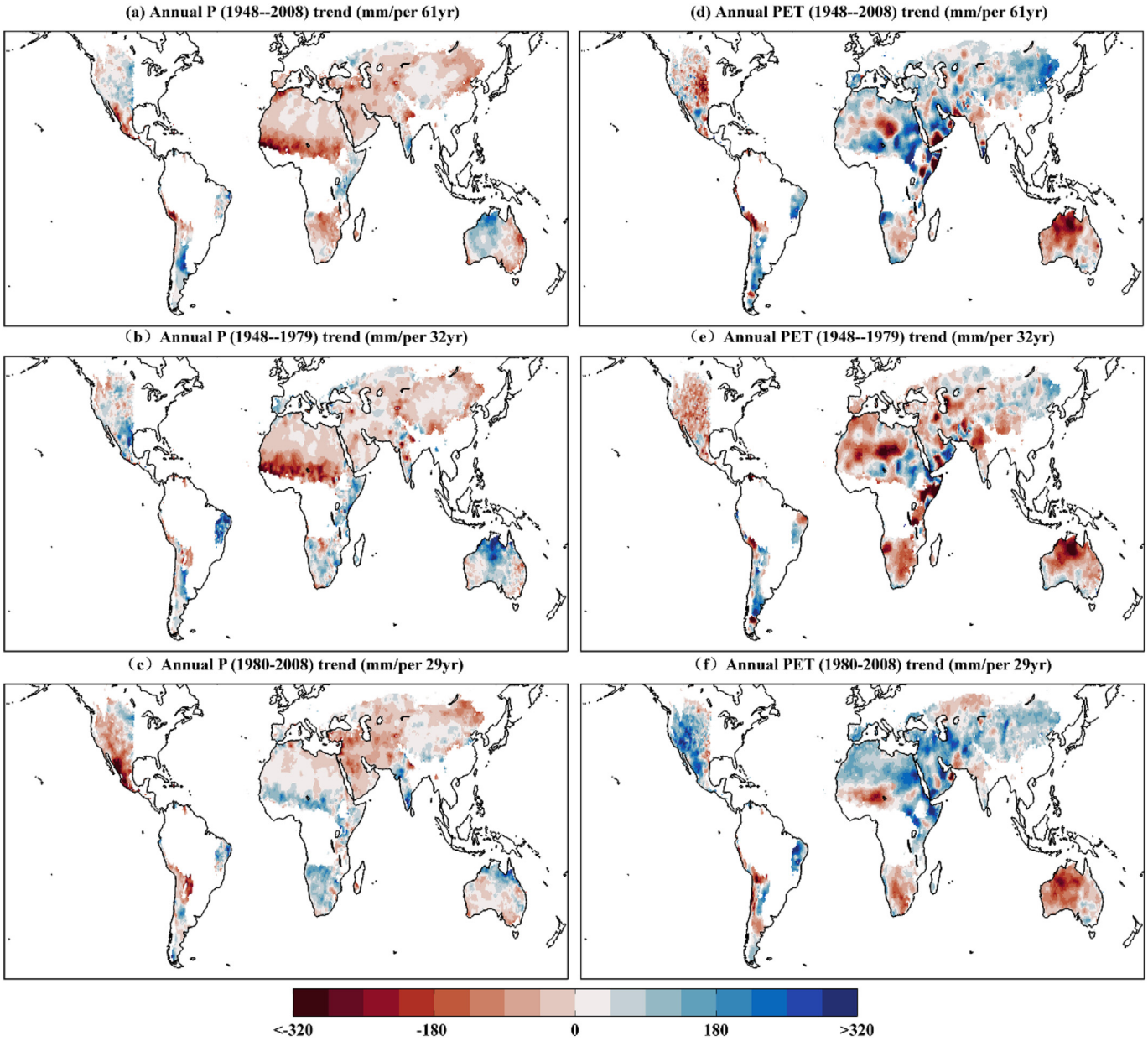

Fig. 7. The linear trend of P and PET (a, d) from 1948 to 2008 (b, e) from 1948 to 1979 (c, f) 1980–2008.

between P/PET and Niño 3.4. The negative areas are mainly located in Australia, Southern Africa, and East Asia, which indicated less precipitation during the El Niño phases but more precipitation during La Niña. In contrast, Central Asia and North America are significantly positive in Niño 3.4.

To quantify the influence degree of PDO, AMO, NAO and Niño 3.4 compared with global warming, a simple five-variable regression equation can be derived to represent the mean P/PET change in the eight main dryland areas using the T, AMO, PDO, NAO, and Niño 3.4 indices as regression variables. From Table 1, the regressed P/PET can capture the variability of the P/PET over East Asia, Central Asia, Northern Africa, North America, and South America. By calculating the contribution of each index, we find that the dynamically induced P/PET played a major role in the P/PET changes in all those eight main dryland areas. Even in dryland of East Asia, the region most affected by global warming, the contribution is only 42.7%. Meanwhile, among those dynamic factors, AMO and PDO played a more important role than other factors.

5. Discussion

5.1. Reassessment of the drought indices' approach

The application of the different indicators has had a decided impact on the study's results. In addition to using P/PET, we have adopted widely used indicators, such as PDSI and SPEI, which all calculate PET according to the Penman-Monteith formula based on physical mechanisms. In comparing the results, we found that the dry/wet pattern shows similarities during 1948–2008 and that only the scope of the significance of the drying or wetting areas is different, especially in the SPEI results. Overall, both PDSI and SPEI accurately express the changes in the dry/wet pattern before and after 1980. Meanwhile, we also compare our result based on different PET datasets from CRU and GLDAS. Fig. S5 showed that our result also not affected by the selected PET data.

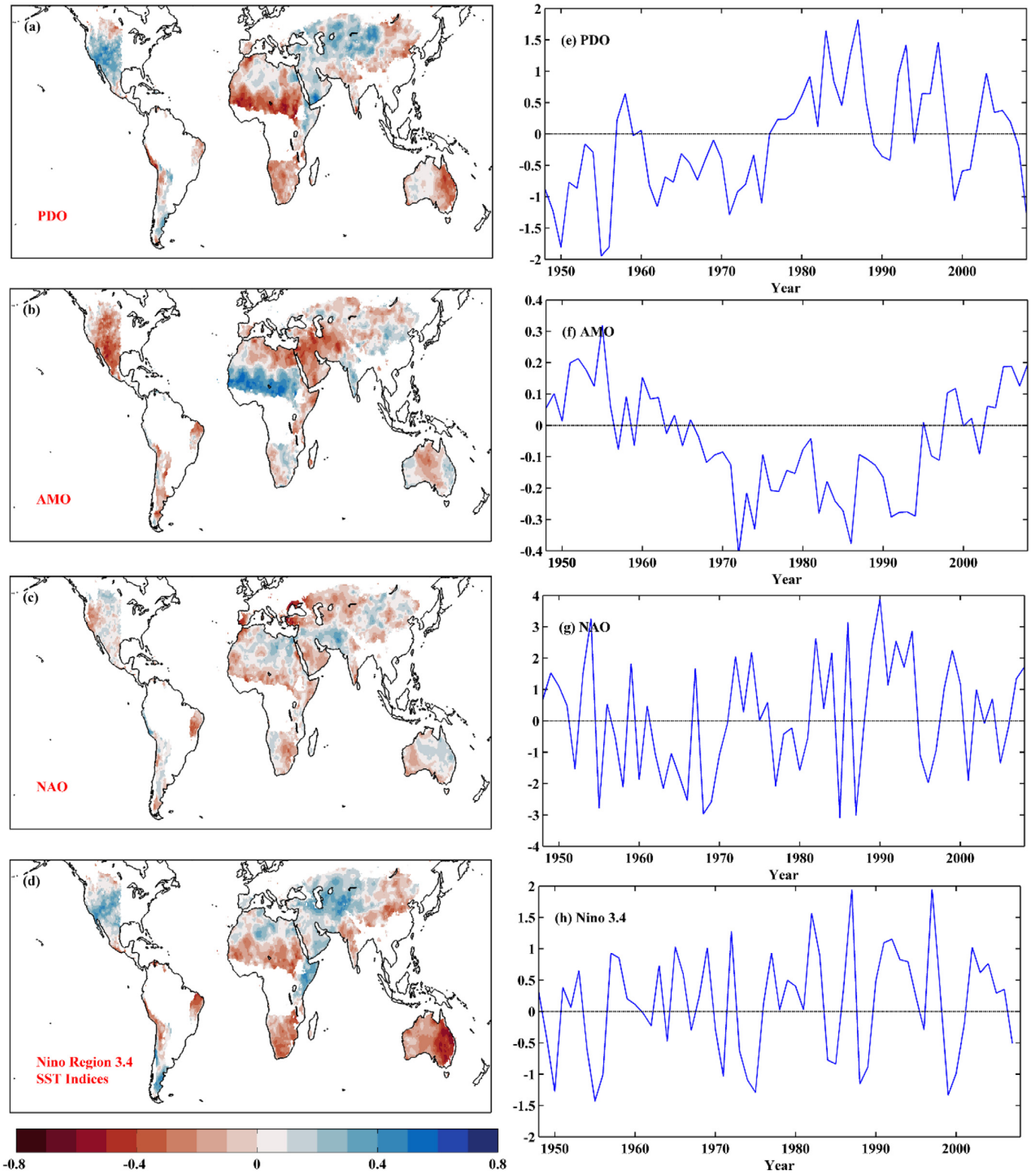

Fig. 8. Time series of the circulation index during 1948–2008 and spatial distribution the correlation coefficients between the circulation index and the P/PET in the period 1948–2008. (a, b) PDO, (c, d) AMO, (e, f) ANO, (g, h) Niño 3.4.

5.2. Comparing with previous results

Our results contradict well-known "dry gets drier and wet gets wetter" paradigms, could be grounded in two main reasons. First, Roderick et al. (2014) found that dry regions would become drier and wet regions wetter only when considering changes in the difference between precipitation and evaporation (P-E). This paradigm was also verified through the distribution of sea surface salinity (Durack et al., 2012) and was therefore quickly adopted by scholars to describe the effects of climate change on global aridity change. However, on land, the P-E was always positive, so this indicator did not apply to land. The second main reason that discounts the "dry to dryer, wet to wetter"

Table 1
The roles of the T, AMO, PDO, NAO, and NAO in the variability of the P/PET for eight different dryland areas.

Region	Formula	*P* value
East Asia	P/PET = -0.598*T + 0.442*AMO + 0.191*PDO + 0.167*NAO-0.004*Niño 3.4	$P < .05$
Central Asia	P/PET = -0.180*T + 0.007*AMO + 0.419*PDO + 0.007*NAO-0.149*Niño 3.4	$P < .05$
Northern Africa	P/PET = -0.457*T + 0.624*AMO-0.132*PDO-0.006*NAO-0.035*Niño 3.4	$P < .05$
North America	P/PET = 0.088*T-0.300*AMO + 0.268*PDO + 0.005*NAO-0.097*Niño 3.4	$P < .05$
South America	P/PET = 0.437*T-0.418*AMO + 0.006*PDO-0.021*NAO + 0.011*Niño 3.4	$P < .05$
Southern Africa	P/PET = -0.113*T + 0.027*AMO-0.225*PDO-0.096*NAO-0.068*Niño 3.4	$P > .05$
West Australia	P/PET = 0.217*T-0.183*AMO-0.079*PDO-0.037*NAO + 0.012*Niño 3.4	$P > .05$
East Australian	P/PET = -0.188*T + 0.030*AMO-0.215*PDO + 0.106*NAO + 0.092*Niño 3.4	$P > .05$

paradigm is that the regional response to climate may differ from global changes, as global warming is adjusted by regional climate change. Based on this fact, Greve et al. (2014) concluded that only 10.8% of global land area was in line with the earlier-cited paradigm, whereas 9.5% of global land area showed dry getting wetter and wet getting drier. These observations were based on > 300 combinations of various hydrological data sets of historical land dryness during 1948–2005.

Even taking differences in method into account, we can find a drying trend in many parts of Africa, especially in the Sahel and eastern Africa, eastern Asia, eastern Australia and northeastern Brazil and a wetting trend mainly located in eastern North America, parts of South America and Australia (Greve et al., 2014). Additionally, Greve et al. (2014) also detected changes in the mean hydroclimatological conditions between the time periods 1948–1968 and 1985–2005. These dry/wet patterns were also similar to our results. From the above analysis, we can see that although dryland areas greatly increased over the past century, the wetting of some dryland areas still occurred.

In addition, the selected time period will have a huge impact on the results. For example, Damberg and Aghakouchak (2014) used SPI data over a 33-year time frame (1980–2012) to show drying/wetting trends around the globe, but their results significantly differed from the findings of Feng and Fu (2013) for the period 1948–2008. This contradiction is mainly reflected in North American and North African drylands. Through investigating the relationship between SST changes and P/PET ratios, our study shows that aridity changes in American and African drylands is attributable to natural precipitation variabilities associated with multi-decadal SST changes, along with large-scale circulation patterns. In these regions, relative to increases in temperature, reductions in precipitation have a greater impact on drought.

5.3. Aridity change driven by natural variability or greenhouse gas forcing?

In a warmer climate, we can easily envisage that aridity would generally increase due to greater potential evaporation that is directly related to the increase in surface heating. In China, for instance, the drylands boundary has extended eastward over Northeast China by about 2° of longitude and 1° of latitude to the south along the middle to lower reaches of the Yellow River (Li et al., 2015). This shift has been caused by decreasing precipitation and enhanced potential evaporation.

However, the aridity change in some regions of drylands is controlled by natural variabilities. For example, in the Sahel region, the identified changes in dryness are unlikely to have been caused by changes in greenhouse gas forcing, because there has been a wetting trend in recent years (Caminade and Terray, 2010), and this wetting may be related to large-scale circulation patterns caused by aerosol forcing and changes in large-scale circulation patterns (e.g., decadal changes in El Niño/Southern Oscillation for tropical rainfall over land) (Hwang et al., 2013). As we know, the climate in the Sahel region is closely related with West African monsoon system, which blows from the tropical Atlantic Ocean across the Sahel and brings rain to this region. Many researches indicated that the historical Sahel drought was induced by warming of the tropical Indian Oceans. During this period, abnormal high pressure centers appeared in around the Sahel for a long time, and the gradient of land-sea low pressure weakened, resulting in the weakening of the monsoon and forming a drying trend (Huang et al., 2015b).

The phase transition of PDO has an important influence on the climate change in western North America (Huang et al., 2015b; Yun et al., 2018). In the middle of 1970s, PDO changed from cold phase to warm phase, namely in the mid latitude North Pacific cooling and the eastern tropical Pacific warming, leading to the Aleutian low deepened and southward, which is conducive to the strengthening of the westerly circulation to bring more warm air into the southwest coast of Mexico and the United States and the temperature is also lower than the normal year in favor of weak PET. Delworth et al. (2015) even concluded that tropical wind anomalies could account for 92% of the simulated drought during the recent decade, with only 8% stemming from anthropogenic radiative forcing changes. The anomalous tropical winds could originate from coupled interactions in the tropical Pacific or from forcing outside the tropical Pacific. Meanwhile, model experiments suggest that the recent tendency toward North American drought would diminish if the tropical winds were to return to climatological conditions. Dai and Zhao (2016) even showed that a large part of the historical drying trend is attributable to decreasing precipitation associated with multi-decadal SST changes in the Pacific and Atlantic Oceans.

Australia bounded by 140°E shows a distinct dry/wet change, which is likely to be affected by the strong warming of the India Ocean in 1970s, affecting the atmospheric circulation in the surrounding areas. The rising air current is favorable to the formation of precipitation in the west of 140 E, while in the east prevalent downdraft leads to reduced precipitation, not only that, the drought will aggravate if occurrence in El Nino year (Huang et al., 2015b).

Indeed, rapid warming since the 1980s has become an increasing important cause of the recent global drying trend. As with every other climate type, drylands climates are impacted by the interaction of climate change and human-induced influences. Furthermore, the projected regional changes in seasonal and annual precipitation vary substantially among the CMIP5 model simulations due to large internal variabilities of precipitation (Feng and Fu, 2013), all of which injects substantial uncertainty into the prediction of aridity change patterns.

6. Conclusion

The changes in dry and wet structures for different spatial and temporal scales during 1948–2008 were studied using the P/PET index, in which P came from multiple datasets and PET was derived from GLDAS. Global dryland areas fluctuated but generally increased, charting a rate of 512,180 km^2/decade since the late 1940s. The most notable feature was the sudden rise in dryland area in the 1980s. From 1980 to 2008, drylands increased by 3.1% (1.90 x $10^6 km^2$) relative to dryland areas during 1948–1979. The expansion of these areas in the 1980s could be explained by increased dryland areas in East Asia ($4.87 \times 10^5 km^2$), Northern Africa ($4.18 \times 10^5 km^2$) and Southern Africa ($2.90 \times 10^5 km^2$).

During the same general time frames of 1948–1979 and 1980–2008,

the dry/wet structure also showed significant differences. Drylands in Northern America, Southern America and Australia showed a wetting trend, whereas the African continent had a significant drought tendency from 1948 to 1979. During 1980–2008, however, the American continent switched to drying while the African continent reversed to wetting. As the same time, Australia's wetting tendency was weakening and East Asia was becoming much drier.

Our results also indicate that the climates across drylands regions were controlled by large-scale circulation patterns (e.g., PDO, AMO), but we did not rule out the potential impact of human activities on climate change in these same area. Overall, our research has provided a scientific basis for an in-depth understanding of changes in drylands within the context of global warming.

Acknowledgments

The research is supported by the Strategic Priority Research Program of the Chinese Academy of Sciences (XDA19030204) and the Science and Technology Service Network Initiative Project of Chinese Academy of Sciences (KFJ-STS-ZDTP-036).

Appendix A. Supplementary data

Supplementary data to this article can be found online at https://doi.org/10.1016/j.gloplacha.2019.04.017.

References

Caminade, C., Terray, L., 2010. Twentieth century Sahel rainfall variability as simulated by the ARPEGE AGCM, and future changes. Clim. Dyn. 35, 75–94. https://doi.org/10.1007/s00382-009-0545-4.

Chen, M., Xie, P.P., Janowiak, J.E., Arkin, P.A., 2002. Global land precipitation: a 50-yr monthly analysis based on gauge observations. J. Hydrometeorol. 3, 249–266. https://doi.org/10.1175/1525-7541(2002)003<0249:GLPAYM>2.0.CO;2.

Cheng, S.J., Huang, J.P., 2016. Enhanced soil moisture drying in transitional regions under a warming climate. J. Geophys. Res.-Atmos. 121, 5391–5398. https://doi.org/10.1002/2015JD024 559.

Dai, A.G., 2011. Characteristics and trends in various forms of the Palmer Drought severity index during 1900–2008. J. Geophys. Res. Atmos. 116, 1248–1256. https://doi.org/10.1002/wcc.81.

Dai, A.G., Zhao, T.B., 2016. Uncertainties in historical changes and future projections of drought, part I: estimates of historical drought changes. Clim. Chang. 144, 1–15. https://doi.org/10.1007/s1058.

Damberg, L., Aghakouchak, A., 2014. Global trends and patterns of drought from space. Theor. Appl. Climatol. 117, 441–448. https://doi.org/10.1007/s00704-013-1019-5.

Delworth, T.L., Zeng, F.R., Rosati, A., Vecchi, G.A., Wittenberg, A.T., 2015. A link between the Hiatus in global warming and North American drought. J. Clim. 28, 3834–3845. https://doi.org/10.1175/JCLI-D-14-00616.1.

Durack, P.J., Wijffels, S.E., Matear, R.J., 2012. Ocean salinities reveal strong global water cycle intensification during 1950 to 2000. Science 336, 455–458. https://doi.org/10.1126/science.1212222.

Feng, S., Fu, Q., 2013. Expansion of global drylands under a warming climate. Atmos. Chem. Phys. 13, 14637–14665. https://doi.org/10.5194/acpd-13-14637-2013.

Greve, P., Orlowsky, B., Mueller, B., Sheffield, J., Reichstein, M., Seneviratne, S.I., 2014. Global assessment of trends in wetting and drying over land. Nat. Geosci. 7, 716–721 (https://doi.org/10.10 38/ngeo2247).

Gutzler, D.S., Kann, D.M., Thornbrugh, C., 2002. Modulation of ENSO-based long-lead outlooks of southwestern US winter precipitation by the Pacific Decadal oscillation. Weather Forecast. 17, 1163–1172. https://doi.org/10.1175/1520-0434(2002)017<1163:MOEBLL>2.0.CO;2.

Hu, Z.Z., Huang, B.H., 2009. Interferential impact of ENSO and PDO on dry and wet conditions in the US Great Plains. J. Clim. 22, 6047–6065. https://doi.org/10.1175/2009JCLI2798.1.

Huang, J.P., Yu, H.P., Guan, X.D., Wang, G.Y., Guo, R.X., 2015a. Accelerated dryland expansion under climate change. Nat. Clim. Chang. 6, 166–171. https://doi.org/10.1038/nclimate2837.

Huang, J., Ji, M., Xie, Y., Wang, S., He, Y., Ran, J., 2015b. Global semi-arid climate change over last 60 years. Clim. Dyn. 46, 1131–1150. https://doi.org/10.1007/s00382-015-2636-8.

Hwang, Y.T., Frierson, D.M.W., Kang, S.M., 2013. Anthropogenic sulfate aerosol and the southward shift of tropical precipitation in the late 20th century. Geophys. Res. Lett. 40, 2845–2850. https://doi.org/10.1002/grl.50502.

Kendall, M.G., 1975. Rank Correlation Methods. Oxford University Press (202 pp).

Legates, D.R., Willmott, C.J., 1990. Mean seasonal and spatial variability in gauge-corrected, global precipitation. Int. J. Climatol. 10, 111–127. https://doi.org/10.1002/joc.3370100202.

Li, Y., Huang, J., Ji, M., Ran, J., 2015. Dryland expansion in Northern China from 1948 to 2008. Adv. Atmos. Sci. 32, 870–876. https://doi.org/10.1007/s00376-014-4106-3.

Mann, H.B., 1945. Nonparametric test against trend. Econometrica 13, 245–259.

Mitchell, T.D., Jones, P.D., 2005. An improved method of constructing a database of monthly climate observations and associated high resolution grids. Int. J. Climatol. 25, 693–712. https://doi.org/10.1002/joc.1181.

Reed, S.C., Coe, K.K., Sparks, J.P., Housman, D.C., Zelikova, T.J., Belnap, J., 2012. Changes to dryland rainfall result in rapid moss mortality and altered soil fertility. Nat. Clim. Chang. 2, 752–755. https://doi.org/10.1038/nclimate1596.

Rodell, M., Houser, P.R., Jambor, U., Gottschalck, J., Mitchell, K., Meng, C.-J., Arsenault, K., Cosgrove, B., Radakovich, J., Bosilovich, M., Entin, J.K., Walker, J.P., Lohmann, D., Toll, D., 2004. The global land data assimilation system. Bull. Am. Meteorol. Soc. 85, 381–394. https://doi.org/10.1175/BAMS-85-3-381.

Roderick, M.L., Sun, F., Lim, W.H., Farquhar, G.D., 2014. A general framework for understanding the response of the water cycle to global warming over land and ocean. Hydrol. Earth Syst. Sci. 18, 1575–1589. https://doi.org/10.5194/hess-18-1575-2014.

Schneider, U., Becker, A., Finger, P., Meyer-Christoffer, A., Rudolf, B., Ziese, M., 2011. GPCC full data reanalysis version 6.0 at 0.5: monthly land-surface precipitation from rain-gauges built on GTS-based and historic data. https://doi.org/10.5676/DWD_GPCC/FD_M_V6_050.

Shi, Y.F., Shen, Y.P., Kang, E., Li, D.l., Ding, Y.j., Zhang, G.W., Hu, R.J., 2007. Recent and future climate change in Northwest China. Clim. Chang. 80, 379–393. https://doi.org/10.1007/s10584-006-9121-7.

Trenberth, K.E., Dai, A.G., Schrier, G.V.D., Jones, P.D., Barichivich, J., Briffa, K.R., 2014. Global warming and changes in drought. Nat. Clim. Chang. 4, 17–22. https://doi.org/10.1038/NCLIMATE2067.

Yun, W., Yu, H., Huang, J., He, Y., Yang, B., Guan, X., Liu, X., 2018. Comparison of the Pacific Decadal Oscillation in climate model simulations and observations. Int. J. Climatol. 38, 99–118. https://doi.org/10.1002/joc.535.